ACS APPLIED MATERIALS & INTERFACES

www.acsami.org Research Article

A Portable Magnetic Particle Spectrometer for Future Rapid and Wash-Free Bioassays

Kai Wu,*,# Vinit Kumar Chugh,# Arturo di Girolamo, Jinming Liu, Renata Saha, Diqing Su, Venkatramana D. Krishna, Abilash Nair, Will Davies, Yongqiang Andrew Wang, Maxim C-J Cheeran,* and Jian-Ping Wang*

Cite This: *ACS Appl. Mater. Interfaces* 2021, 13, 7966−7976 Read Online

ACCESS | Metrics & More | Article Recommendations | Supporting Information

ABSTRACT: Nowadays, there is an increasing demand for more accessible routine diagnostics for patients with respect to high accuracy, ease of use, and low cost. However, the quantitative and high accuracy bioassays in large hospitals and laboratories usually require trained technicians and equipment that is both bulky and expensive. In addition, the multistep bioassays and long turnaround time could severely affect the disease surveillance and control especially in pandemics such as influenza and COVID-19. In view of this, a portable, quantitative bioassay device will be valuable in regions with scarce medical resources and help relieve burden on local healthcare systems. Herein, we introduce the MagiCoil diagnostic device, an inexpensive, portable, quantitative, and rapid bioassay platform based on the magnetic particle spectrometer (MPS) technique. MPS detects the dynamic magnetic responses of magnetic nanoparticles (MNPs) and uses the harmonics from oscillating MNPs as metrics for sensitive and quantitative bioassays. This device does not require trained technicians to operate and employs a fully automatic, one-step, and wash-free assay with a user friendly smartphone interface. Using a streptavidin-biotin binding system as a model, we show that the detection limit of the current portable device for streptavidin is 64 nM (equal to 5.12 pmole). In addition, this MPS technique is very versatile and allows for the detection of different diseases just by changing the surface modifications on MNPs. Although MPS-based bioassays show high sensitivities as reported in many literatures, at the current stage, this portable device faces insufficient sensitivity and needs further improvements. It is foreseen that this kind of portable device can transform the multistep, laboratory-based bioassays to one-step field testing in nonclinical settings such as schools, homes, offices, etc.

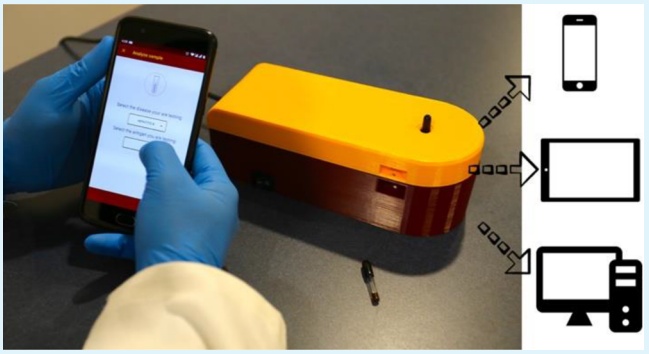

KEYWORDS: *point-of-care, wash-free, bioassay, magnetic particle spectrometer, portable*

1. INTRODUCTION

The past decade has seen the continuous advancing of disease diagnostic platforms in a wide variety of research areas such as magnetic, optical, mechanical, and electrochemical sensing systems.[1−13] However, the processes of developing these platforms toward point-of-care (POC) devices for field testing are largely delayed despite their promising high sensitivity.[14−16] Most of the diagnostic platforms are complicated to use on-site since they rely on expensive and/or bulky laboratory equipment as well as on trained technicians to operate. Furthermore, biological samples often need to be preprocessed to remove substances such as blood cells from whole blood samples that may interfere with the fluorescence signal. These factors lead to relatively expensive diagnostics and long turnaround time. Although there are strip tests available in the market for at-home pregnancy and common diseases testing that are easy to use and inexpensive,[17,18] these strip tests are only limited to certain diseases and there is a big concern raised by researchers on the accuracy such as high false positive rates.[19,20] Furthermore, the strip test results are often qualitative (or binary), which limits their capability for daily monitoring of chronic disease and in-depth disease analysis.

In recent years, the demand for high accuracy, inexpensive, and easy-to-use POC devices for routine daily diagnostics that are more accessible to patients is tremendously increasing. During the COVID-19 pandemic, the inaccessibility to portable diagnostic devices has put great pressure on the local healthcare systems especially in developing countries and

Received: November 25, 2020
Accepted: February 4, 2021
Published: February 10, 2021

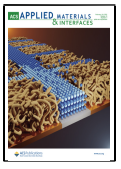

https://dx.doi.org/10.1021/acsami.0c21040
ACS Appl. Mater. Interfaces 2021, 13, 7966−7976

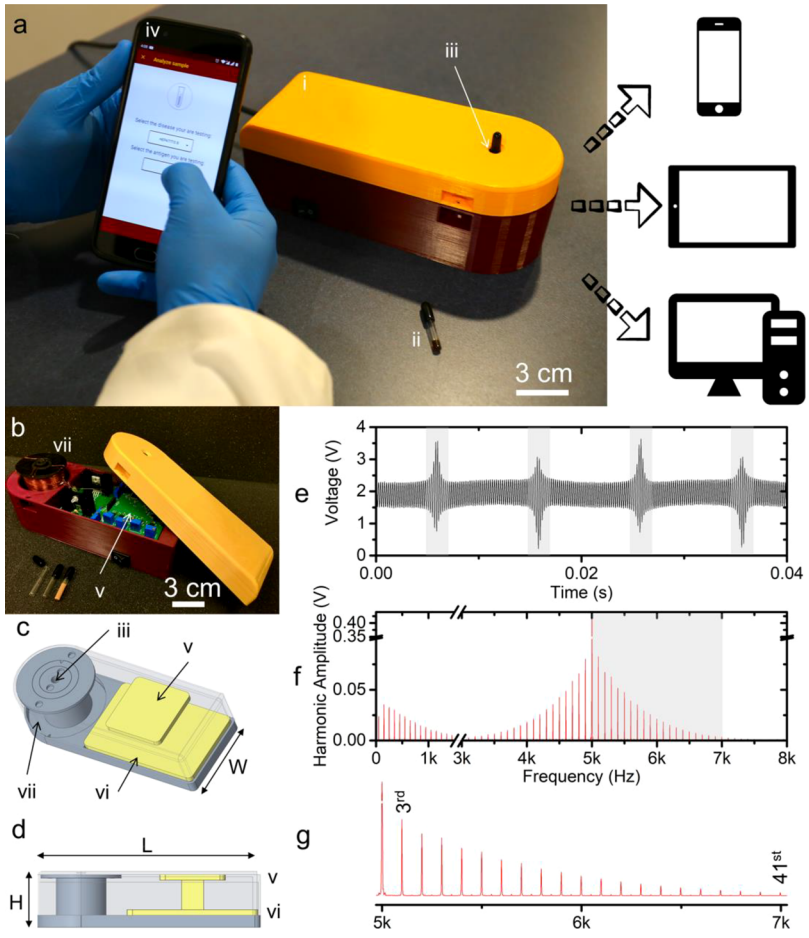

Figure 1. (a) Photograph of the MagiCoil portable device with a smartphone application. The overall dimensions of device are 212 mm (L) × 84 mm (W) × 72 mm (H). (i) Device shell is 3D printed using the material. (ii) Disposable, USP type I glass vial containing the MNP sample. (iii) Sample loading port. (iv) Smartphone application. (b) Photograph of the internal structures of the MagiCoil device. (c) 3D model of the MagiCoil device with (v) top and (vi) bottom circuit boards, and (vii) three sets of copper coils for generating magnetic driving fields and collecting dynamic magnetic responses of MNPs. (d) Side view of the 3D model with length (L) and height (H) labeled. (e) Discrete time voltage signal collected from pick-up coils during two periods of low-frequency field. The dynamic magnetic responses of MNPs cause visible spikes as highlighted in gray regions. (f) Frequency domain MPS spectra from (e). Higher harmonics are observed. (g) Enlarged view of higher harmonics (the 3rd to the 41st harmonic) between 5 and 7 kHz. More details on the 3D models and user interfaces are given in the Supporting Information, S1.

rural areas.[21−24] Diagnostic platforms that combine the accessibility of strip tests and the high accuracy and quantitative nature of laboratory-based tests will greatly change current situation.

Herein, we introduce a portable, quantitative diagnostic platform based on a magnetic particle spectrometer (MPS) called as MagiCoil, that can be operated by a layperson in nonclinical settings such as schools, homes, and offices, etc., without much training requirements. This technique relies on detecting dynamic magnetic responses of magnetic nanoparticles (MNPs) from biological samples.[10,25−33] Since MNPs are the sole sources of magnetic signal and most biological samples are non-magnetic or paramagnetic, this MPS platform is naturally immune to the background noise from biological samples, and thus, it does not require sample pre-processing and allows one-step and wash-free bioassays. Furthermore, by surface functionalizing MNPs with different ligands (e.g., carboxylic acid and amine), nucleic acids (i.e., DNA and RNA), and proteins (e.g., antibodies, streptavidin, protein A, etc.), the MNPs can be specifically modified for detecting different target analytes as well as diseases.[10,28,29,31,34−36] Recently, it has been reported that a custom-built scanning MPS is used for biomolecule imaging, showing great potential for disease diagnostics and imaging.[37]

2. EXPERIMENTAL SECTION

2.1. MagiCoil Portable Device. Figure 1a shows a photograph of the developed MagiCoil portable device along with a smartphone application user interface. The overall dimensions of this device are 212 mm (L) × 84 mm (W) × 72 mm (H). It is powered by wall plug and can communicate with smartphones (Android and IOS systems), tablets, computers through Bluetooth and USB.[38] The device shell (Figure 1a-i) is 3D printed with a polylactic acid (PLA) material. The biofluid sample holder is a flat bottom, USP type I, glass vial with dimensions of 31 mm × 5 mm and a volume capacity of 0.25 mL (Figure 1a-ii). This kind of a glass vial is one-time use only and disposable and it can be seamlessly inserted into the sample loading port (Figure 1a-iii) from the top of the MagiCoil device. The user interface (Figure 1a-iv) gives users step-by-step instructions on carrying out the testing. Figure 1b shows the photograph of two circuit boards and three sets of copper coils for generating magnetic fields as well as collecting dynamic magnetic responses of MNPs. MagiCoil portable device 3D models are shown in Figure 1c,d. The top circuit board (Figure 1c-v) is the signal readout board and consists of instrumentation amplifier, bandpass filters, and ADC stages. A microcontroller unit is also housed on the same board to

https://dx.doi.org/10.1021/acsami.0c21040
ACS Appl. Mater. Interfaces 2021, 13, 7966−7976

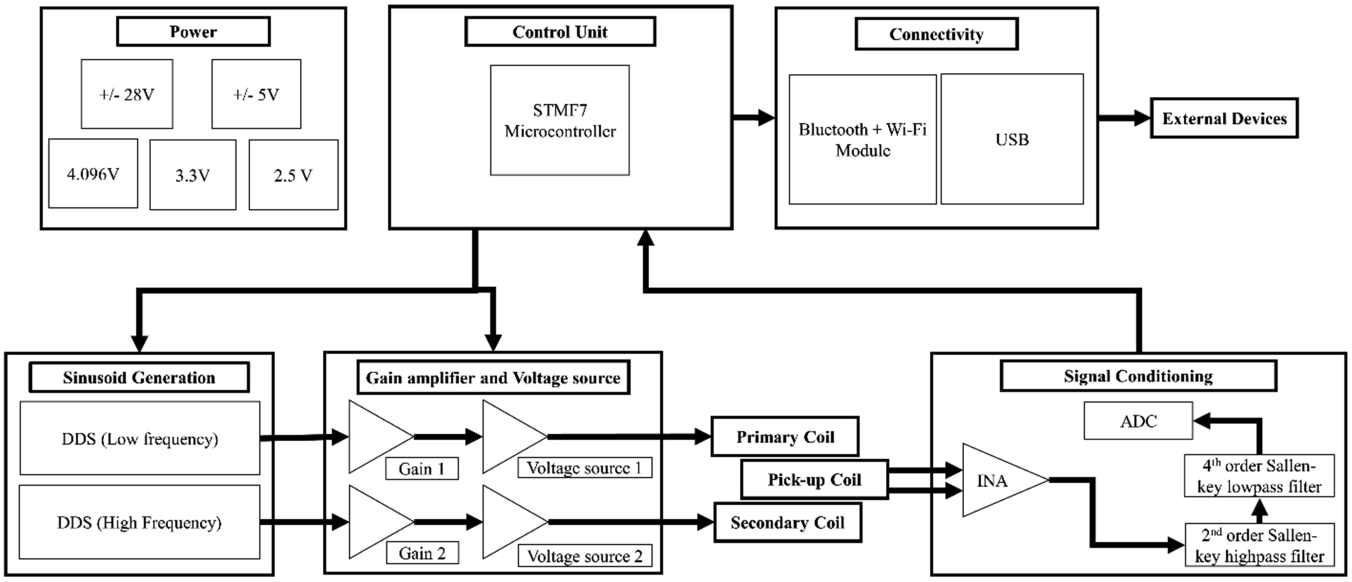

Figure 2. Block diagram of MagiCoil portable device circuit design.

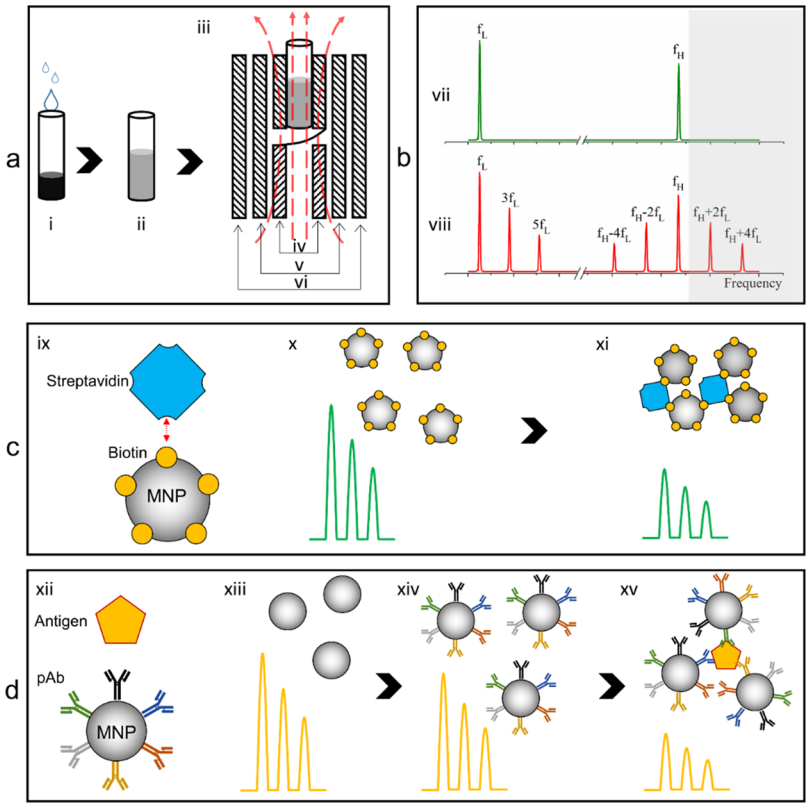

Figure 3. (a) General steps of carrying one bioassay on the MagiCoil portable device. (b) MPS spectra collected from samples (vii) with loaded MNPs and (viii) without loaded MNP. (c) Schematic drawing of MPS-based biotin-streptavidin detection. (d) Schematic drawing of MPS-based antibody−antigen detection.

communicate with ADC circuitry. The bottom circuit board (Figure 1c-vi) consists of mainly power generation ICs and coil driver circuit to generate the required magnetic fields.

2.2. Circuit Design of the MagiCoil Portable Device. Figure 2 shows the block level breakdown of the developed MagiCoil device. One of the key requirements for MagiCoil modality for bioassay applications is the generation of phase stable magnetic fields. DDS IC from Analog Devices AD9833 is used to generate stable low-frequency (f_L) and high-frequency (f_H) sinusoid fields for this application. Frequencies f_L and f_H are kept at 50 Hz and 5 kHz, respectively. DC-shift and gain stages are implemented to obtain suitable signal amplitudes using ultrahigh precision operational amplifiers OPA189 before feeding the signal to voltage source implementation using a high-voltage, high-current operational amplifier from Texas Instruments (TI) OPA548. For the application presented in this work, the magnitude of low-frequency field is kept at 250 Oe and that of the high-frequency field is kept at 25 Oe. At its current stage, the MagiCoil device operates from an external wall adapter, which supplies +28 V to the device. The successive voltages are generated onboard using various power supply ICs. LTC7149

https://dx.doi.org/10.1021/acsami.0c21040
ACS Appl. Mater. Interfaces 2021, 13, 7966−7976

Table 1. Summary on Five Types of Iron Oxide MNPs

sample index	concentration (mg/mL)	surface	H_c (Oe)[a]	M_s (@ 2000 Oe)[a,b]	M (@ 300 Oe)[a,c]	A3 (μV)[d]	A3/μg MNP (μV/μg)[e]
A: SHB30	0.8	biotin	±24.5	68.3 emu/g	59.3 emu/g	5067	79.2
				54.6 μemu/μL	47.4 μemu/μL		
B: SHB30	3	biotin	±74.1	33.5 emu/g	14.8 emu/g	4169	17.4
				100.5 μemu/μL	44.4 μemu/μL		
C: SHP30	17.5	carboxylic	±22.4	63.1 emu/g	49.2 emu/g	81,630	58.3
				1104.3 μemu/μL	861μemu/μL		
D: MP25 BN	1−2	biotin	±13.4	26.3−52.7 emu/g	14.7−29.4 emu/g	1924	12.0−24.0
				26.3−105.4 μemu/μL	14.7−58.8 μemu/μL		
E: MP25 CA	2	carboxylic	±15.9	17.6 emu/g	9.5 emu/g	1639	10.2
				35.2 μemu/μL	19 μemu/μL		

[a]VSM results are given in the Supporting Information, S2. [b]The saturation magnetization of each MNP sample is obtained under a magnetic field of 2000 Oe. [c]The specific magnetization of each MNP sample is obtained under a magnetic field of 300 Oe. [d]MPS 3rd harmonic amplitude. [e]MPS 3rd harmonic amplitude per microgram of iron oxide MNP.

from Analog Devices is used for generating −28 V, TL751 and LTC1983 are used for generating +5 V and −5 V, respectively, and 4.096, 3.3, and 2.5 V are generated using LTC6655, TPS62177, and LT3060, respectively. In the future, we do plan to have an on-board battery setup to meet the power requirements.

The parameters of coils used in the MagiCoil portable device are primary coil: 1278 turns (23 AWG copper wire), secondary coil: 449 turns (30 AWG copper wire), and pick-up coil: 755 turns on each side of the balanced coil (36 AWG copper wire). Differential voltage signal generated form balanced pick-up coils (Figure 3a: iv) is amplified using an instrumentation amplifier by TI INA128. Sallen-Key implementation of high-pass and low-pass filters are used for signal-to-noise-ratio (SNR) improvement followed by a DC-shift stage, all implemented using the operational amplifiers OPA189. A 24-bit pseudo-differential amplifier by Linear Technology LTC2368-24 is used to sample the filtered signal. STM32F767 from STMicroelectronics is the choice of a microcontroller this application enabling communication of real-time sampled data at 316 kSPS with on-board ADC.

For each round of bioassay, the MagiCoil device records 170,000 samples, which has an effective time of only 0.54 s. Real-time communication of the sampled data with laptop is handled using a custom Python script utilizing USART protocol. FTDI cable TTL-232RG is utilized to enable this communication between the desktop and on-board microcontroller. The discrete time voltage signal collected from one MNP sample is shown in Figure 1e during two periods of the low-frequency field. Visible spikes due to the dynamic magnetic responses of MNPs are highlighted in gray regions. These spikes are responsible for the higher harmonics in MPS spectra, as shown in Figure 1f. Zoom-in view of the 3rd to the 41st harmonics between 5 and 7 kHz are also shown in Figure 1g. At the current stage, the post processing of the collected discrete time voltage signal is handled by MATLAB.

2.3. Detection Steps on the MagiCoil Portable Device. Figure 3a shows the general steps of carrying out one bioassay on the portable device. A biofluid sample containing target biomolecules is dropped into a glass vial, which is preloaded with a fixed amount of MNPs (Figure 3a-i). The mixture is incubated at room temperature on a plate shaker for a fixed amount of time (Figure 3a-ii) to allow the specific binding. Then, the glass vial is inserted into the sample loading port for data collection (Figure 3a-iii). Each round of MPS measurement takes less than 1 s (specifically, 0.54 s) and to ensure that the coils do not get heated during the measurements, a gap of 3 min is taken between any successive readings.

2.4. MPS-Based Bioassay Detection Mechanism. The MagiCoil data collection part consists of three sets of copper coils: a pair of differentially wound pick-up coils (Figure 3a-iv), one set of high-frequency field f_H driving coil (Figure 3a-v), and one set of low-frequency field f_L driving coil (Figure 3a-vi). Figure 3b shows a typical MPS spectra pattern collected from samples with loaded MNPs (Figure 3a-vii) and without loaded MNP (Figure 3a-viii). Under the application of oscillating magnetic fields, the magnetic moments of MNPs rotate along the external magnetic field direction, this process generate dynamic magnetic responses that can be detected by the pick-up coils.[39−42] As a result, MNPs generate higher harmonics that are observed from the MPS spectra. In the results reported in this work, we only analyze the higher harmonics at $f_H + 2f_L$ (the 3rd harmonic), $f_H + 4f_L$ (the 5th harmonic), $f_H + 6f_L$ (the 7th harmonic), $f_H + 8f_L$ (the 9th harmonic), $f_H + 10f_L$ (the 11th harmonic), $f_H + 12f_L$ (the 13th harmonic), and $f_H + 14f_L$ (the 15th harmonic) as highlighted in the gray region in Figure 3b. It is worth mentioning that most of the previous research works rely on the 3rd and the 5th harmonics as metrics for quantitative bioassays. Herein, we used higher order harmonics (from the 3rd up to the 15th harmonics) as reliable metrics to achieve highly sensitive and quantitative bioassay purposes.

Taking the streptavidin detection as an example, as shown in Figure 3c-ix, streptavidin is a homo-tetramer with an extraordinarily high affinity for biotin, 1 mol of streptavidin can bind with 4 mol of biotin. Well-dispersed biotinylated MNPs show high dynamic magnetic responses to external oscillating fields as well as large harmonic amplitudes (Figure 3c-x). However, in the presence of streptavidin, biotinylated MNPs will cross-link and form clusters (Figure 3c-xi) on streptavidin homo-tetramers. The clustering of MNPs weakens the dynamic magnetic responses, and as a result, the harmonic amplitudes drop. This difference in harmonic amplitude reduction can be used to quantitatively analyze the amount and concentration of streptavidin in the sample.

Compared to most bioassay techniques, this MPS-based bioassay does not require removing unbound target analytes, making it a wash-free, one-step testing that is accessible by a layperson in nonclinical settings.

In addition, this kind of an MPS platform can be customized to detect a wide range of biomarkers as well as diseases. A more generalized detection scheme for detecting antigens using antibody−antigen interactions is shown in Figure 3d-xii. MNPs can be surface functionalized with polyclonal antibodies (pAb). In the presence of target antigens, these pAb will specifically bind to different epitopes from the antigens.[10,28] Thus, this cross-linking causes clustering of MNPs. As a result, the hydrodynamic size of MNPs gradually increases after the surface conjugation of pAb (Figure 3d-xiii,xiv) and after the cross-linking in the presence of target antigens (Figure 3d-xiv,xv). Similarly, this cross-linking caused MNP clustering weakens the dynamic magnetic responses, and the harmonic amplitudes drop, although there is no theoretical evidence showing which higher harmonic is more sensitive to the binding events of MNPs to target analytes.

3. MATERIALS AND METHODS

3.1. Materials. The iron oxides MNPs used in this work are SHB30 and SHP30 provided by Ocean Nano Tech LLC, and MP25 BN and MP25 CA are purchased from Nanocs Inc. The streptavidin

https://dx.doi.org/10.1021/acsami.0c21040
ACS Appl. Mater. Interfaces 2021, 13, 7966−7976

(product no. S4762) and phosphate-buffered saline (PBS, product no. 79378) are purchased from Sigma-Aldrich Inc. Streptavidin is a salt-free, lyophilized powder with a biotin-binding capacity of 4 mol/mol (biotin) and a molecular weight (MW) of ∼60 kDa. A sample holder is a 0.25 mL flat bottom glass vial with dimensions 31 mm × 5 mm, USP type I, manufactured by ALWSCI Technologies Co., Ltd. Round rubber end caps of 5 mm inner diameter and 15 mm height are used to seal a sample holder to prevent liquid sample spill, manufactured by Uxcell.

3.2. Static (dc) Hysteresis Loop Measurement. For each MNP liquid suspension, 10 μL of sample is drawn using a pipette and dropped on a parafilm. The droplet is dried under N_2 at room temperature. The dc hysteresis loops of samples A−E (listed in Table 1) are measured at 300 K using a physical properties measurement system (PPMS) integrated with a vibrating sample magnetometer (Quantum Design), as plotted in Figure S2 in the Supporting Information. The magnetic field is swept from −2000 Oe to +2000 Oe with a step of 2 Oe (or −300 Oe to +300 Oe with a step of 1 Oe), and the averaging time for each step is 100 ms. The dc magnetic properties of MNPs such as coercivities and saturation magnetizations are listed in Table 1.

3.3. Particle Hydrodynamic Size Measurement. The hydrodynamic size distribution of the MNP sample is characterized using a dynamic light scattering (DLS) particle tracking analyzer (model: Microtac Nanoflex). One hundred fifty microliters of samples I, III, V, VII, and X (listed in Table 2) is diluted in 1.35 mL of PBS, reaching a total sample volume of 1.5 mL of mixture. This is followed by ultrasonication for 30 min before the DLS characterization.

Table 2. Samples of Varying Amount of Iron Oxide MNPs

sample index	MNP concentration (nM)	MNP concentration (mg/mL)	MNP weight (μg)
1	27.2	0.8	64
2	13.6	0.4	32
3	6.8	0.2	16
4	3.4	0.1	8
5	1.7	0.05	4
blank	0	0	0

4. RESULTS AND DISCUSSION

4.1. Characterization of Different Types of MNPs. Five types of MNPs with varying sizes, concentrations, magnetic properties, and surface modifications are first characterized on our MagiCoil portable device. Samples A−C are iron oxide nanoparticles with an average magnetic core size of 30 nm. Samples D and E are iron oxide nanoparticles with an average magnetic core size of 25 nm. MNPs from samples A, B, and D are coated with biotin, while MNPs from samples C and E are coated with carboxylic. These different surface coating layers act as reactive groups and improve the colloidal stability of MNP suspensions. As a result, the coating layers increase the hydrodynamic size of MNPs by ∼10 nm. Eighty microliters of MNP suspension is drawn to a glass vial for MPS measurements. As a comparison, the standard dc hysteresis loop measurements are carried out. From the dc hysteresis loop results in the Supporting Information, S2, the saturation magnetization of MNPs, M_s (unit: emu/g), are ranked as: A > C > B ∼ D > E. Due to the varying concentrations of MNPs in each sample, the magnetic moment per volume of suspension is calculated and listed in Table 1. It should be noted that although all MNPs are iron oxide nanoparticles, their saturation magnetizations are different due to different ratios of γ-Fe_2O_3, Fe_3O_4, and α-Fe_2O_3 materials used for synthesizing the magnetic cores. Sample C with the highest MNP concentration yields highest magnetic moment per microliter volume (unit: μemu/μL). The magnetic moment per volume of MNPs from highest to lowest are ranked as: C > A > B ∼ D > E. All the MNP samples show negligible coercivities.

Nine independent MPS measurements are carried out on each sample, and the averaged harmonic amplitudes (3rd, 5th, 7th, 9th, 11th, 13th, and15th) are summarized in Figure 4a.

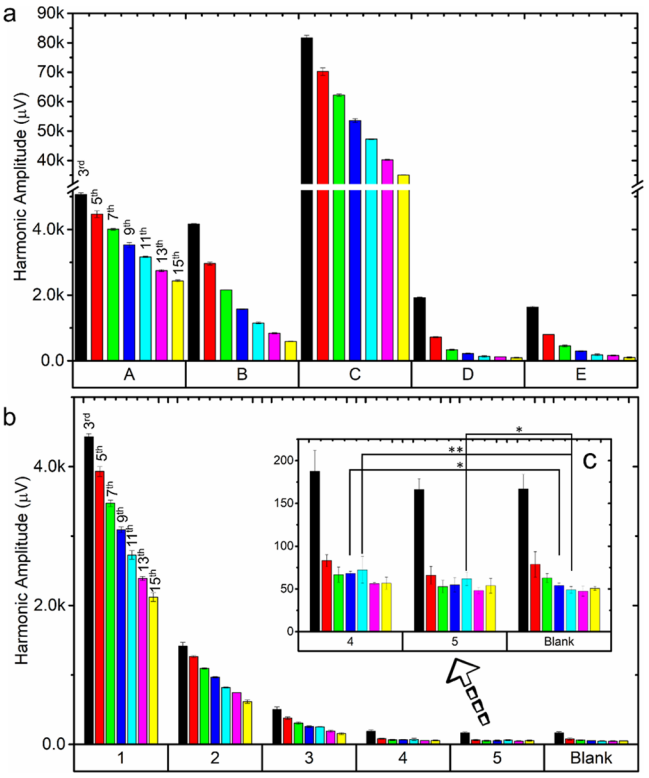

Figure 4. (a) MPS harmonics of five different types of MNPs: A−E, monitored by the MagiCoil portable device. (b) MPS harmonics of varying amount of SHB30 iron oxide MNPs, monitored by the MagiCoil portable device. ** $p < 0.01$, * $p < 0.05$. (c) Zoom-in view of harmonics from samples 3, 4, and blank with p-values labeled. Error bars represent standard deviations. The p-values for the 3rd to the 15th harmonics of samples 4 and 5 to blank sample are listed in S3 in the Supporting Information.

Harmonic amplitudes from highest to lowest are ranked as: C > A > B > D > E, which agrees with the dc hysteresis loop measurements of magnetic moment per volume of MNP suspension. In addition, these higher harmonics are caused by the nonlinear magnetic responses of MNPs under ac magnetic fields. Thus, the degree of nonlinearity in the hysteresis loops under an external magnetic field of −300 Oe to +300 Oe (Figure S2f−j) also explains the higher harmonic amplitudes in samples A and C and lower harmonic amplitudes in samples D and E. Since the hydrodynamic sizes of MNPs from samples A−E are similar, the MNP amount/concentration and the nonlinearity of magnetization curves directly cause the different magnetic responses and different magnitudes of higher harmonics.

We listed the averaged 3rd harmonic amplitude from each sample in Table 1 for comparison. The 3rd harmonic amplitude shows a similar trend with respect to the magnetic moment per volume of sample at 300 Oe. In addition, the calculated 3rd harmonic amplitude per microgram of iron

https://dx.doi.org/10.1021/acsami.0c21040
ACS Appl. Mater. Interfaces 2021, 13, 7966−7976

oxide MNP is also listed in Table 1, which shows a similar trend with respect to the specific magnetizations under a magnetic field of 300 Oe.

4.2. Minimum Amount of Iron Oxide MNPs Detectable by the MagiCoil Portable Device. To demonstrate the sensitivity of our MagiCoil portable device in detecting the lowest amount of iron oxide MNPs, 80 μL of SHB30 iron oxide MNP samples are prepared by two-fold dilutions, as listed in Table 2. From samples 1 to 5, the MNP weight per vial drops from 64 to 4 μg. Sample index blank is a glass vial containing 80 μL of PBS. As shown in Figure 4b, the higher harmonics from samples 1−5 are summarized and compared with the blank sample. It is clearly seen that sample 1 shows highest MPS signals followed by samples 2 and 3, Although samples 4 and 5 show similar harmonic amplitudes compared to blank sample as shown in Figure 4c, the two-sample t test results show that the 9th and the 11th harmonics from sample 4 are significantly different from the blank sample, with p-values of 0.034 and 0.01, respectively. In addition, the 11th harmonic from sample 5 is significantly different from the blank sample, showing a p-value of 0.04. Thus, we can conclude that our MagiCoil portable device can detect as low as 4 μg of iron oxide MNPs. The calculated lowest detectable magnetic moment by this portable device is 273.2 μemu, signal from blank sample.

4.3. MagiCoil Portable Device for Streptavidin Detection. Herein, the capability of our MagiCoil portable device for bioassay applications is demonstrated by using a streptavidin-biotin binding system. Since sample A shows the highest MPS harmonic amplitude per microgram of iron oxide MNP, which allows for bioassays with minimum amount of MNPs per test, and thus, herein, we choose SHB30 from sample A for the streptavidin detection. Eighty microliters of 1 mg/mL SHB30 iron oxide MNPs are mixed with varying concentrations/amounts of 80 μL of streptavidin protein. As shown in Table 3, samples I−IX are prepared by twofold dilution of streptavidin, with streptavidin concentrations varied from 2048 nM down to 8 nM. Sample X is prepared by mixing 80 μL of 1 mg/mL SHB30 iron oxide MNPs with 80 μL of PBS. The MNP to streptavidin ratios are also listed in Table 3. All the samples are incubated at room temperature for 30 min to allow the binding of streptavidin molecules to biotins from the MNP surface.

Table 3. Samples of Varying Amounts of Streptavidin

sample index	streptavidin concentration (nM)	MNP:streptavidin ratio
I	2048	1:60
II	1024	1:30
III	512	1:15
IV	256	1:7.5
V	128	1:3.75
VI	64	1:1.88
VII	32	1:0.94
VIII	16	1:0.47
IX	8	1:0.24
X	0	

We carried out six independent MPS measurements on each sample, as shown in the scatter plots in Figure 5a. Two-sample t test is carried out on each sample to compare with the control group (sample index X, 0 nM). As shown in Figure 5a, the 3rd harmonic amplitudes from samples I−V are significantly different from the control sample X with p-values smaller than 0.05. However, the 3rd harmonics from samples VI−IX are not significantly different from the control sample X with p-values larger than 0.05. Thus, based on the 3rd harmonic as the sole metric, the detection limit of our MagiCoil portable device for streptavidin is 128 nM (equal to 10.24 pmole).

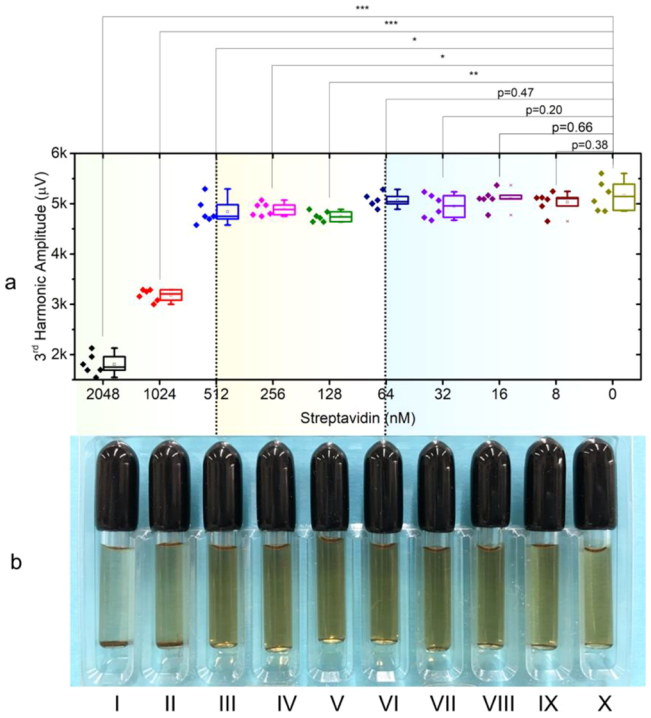

Figure 5. (a) Box plots of the 3rd harmonics from samples I−X with varying amounts of streptavidin. Two-sample t test is carried out on each sample compared with sample X (control group). (b) Photographs of samples I−X showing different degrees of MNP clustering caused by streptavidin. *** $p < 0.001$, ** $p < 0.01$, * $p < 0.05$. Box plots of the 5th and the 7th harmonics from samples I−X along with p-values are given in the Supporting Information, S4.

Figure 5b shows the photograph of samples I−X after the 30 min of incubation. Precipitates are observed from samples I (2048 nM) and II (1024 nM), and the supernatants are clearer due to decreased amount of MNPs left in the solution, which indicates that larger amount of streptavidin proteins (MNP:streptavidin ratios of 1:60 and 1:30) are causing the MNPs to form clusters. Due to the cross-linking of MNPs and streptavidin, MNPs are closely compacted and their hydrodynamic sizes dramatically increase. As a result, the Brownian relaxation of bound MNPs is blocked and their dynamic magnetic responses become weaker.

The dynamic size of MNPs (and MNP clusters) from samples I, III, V, VII, and X are measured on a DLS system. As shown in Figure 6a,b, samples X (0 nM, control group) and VII (32 nM) are showing very similar size distributions both with particle size peaks at ∼50 nm, indicating that small amount of streptavidin in sample VII cannot effectively increase the hydrodynamic sizes of MNPs. Furthermore, the two-sample t test on samples VII and X shows that there is no significant change of MNP hydrodynamic size ($p = 0.96$).

As we increase the amount of streptavidin, the distribution of particle sizes becomes wider and particles with several hundreds and thousands of nanometers' sizes are observed. The two-sample t test on samples V and X shows a p-value of

https://dx.doi.org/10.1021/acsami.0c21040
ACS Appl. Mater. Interfaces 2021, 13, 7966−7976

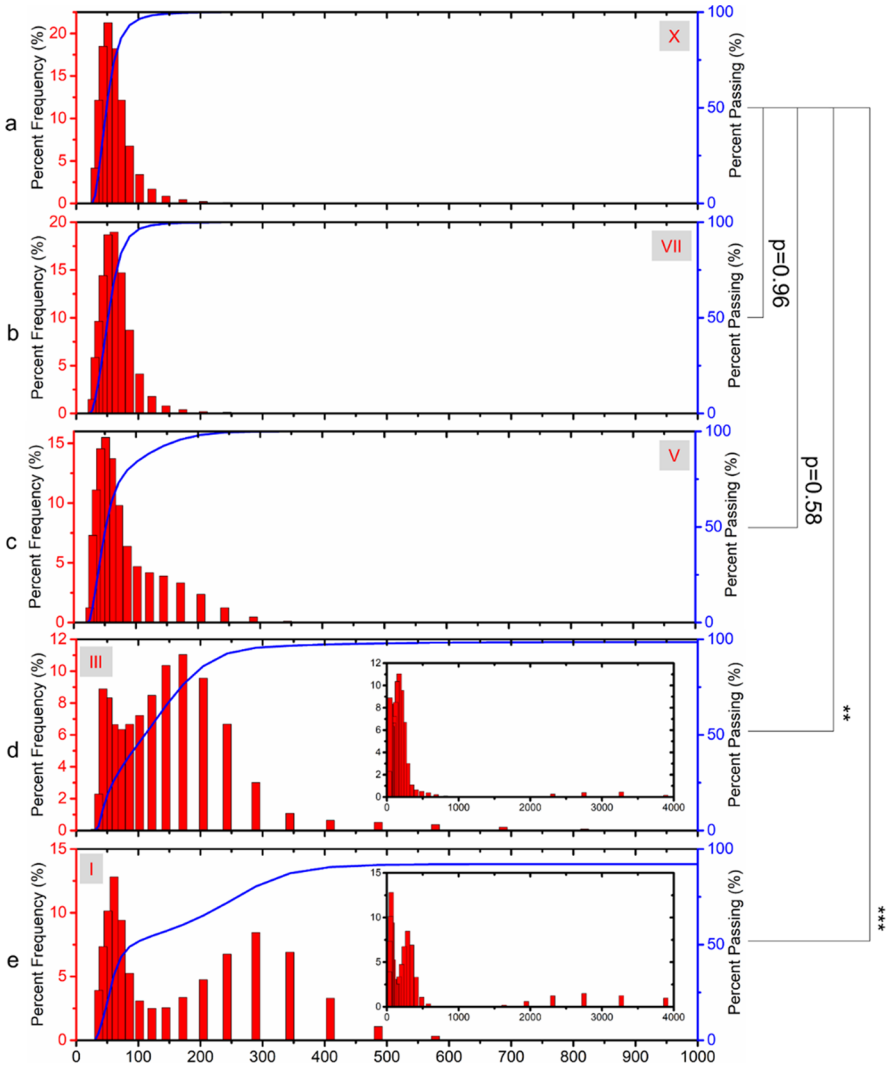

Figure 6. Hydrodynamic size distributions of MNPs from samples (a) X (control group, 0 nM), (b) VII (32 nM), (c) V (128 nM), (d) III (512 nM), and (e) I (2048 nM) measured by DLS. *** $p < 0.001$, ** $p < 0.01$, * $p < 0.05$.

0.58 and this small difference can be explained by the peak tail in Figure 6c within a size range of 100−300 nm. From sample III in Figure 6d, we observed a second particle size peak at ∼175 nm. On the other hand, a second particle size peak is also observed at ∼300 nm from sample I in Figure 6e. The insets in Figure 6d,e show that larger particles with several thousand nanometers size are present in samples I and III, proving that the higher concentration/amount of streptavidin is causing MNP cross-linking and clustering. As a result, the increased hydrodynamic size weakens the dynamic magnetic responses and lower MPS harmonic amplitudes are detected from the MagiCoil portable device.

Figure 7a shows the 3rd to the 15th harmonics from samples I to X. For each sample, harmonic amplitudes drop as harmonic index increases but still above the noise floor. Due to the larger amount of streptavidin in the samples, samples I and II show significantly lower harmonic amplitudes than other samples. Furthermore, we summarized the higher harmonic amplitudes (the 3rd to the 15th harmonics) of samples I−X from six independent MPS measurements. Then, we applied two-sample t test to compare the i^{th} harmonics of sample j to the i^{th} harmonics of sample X, where i = 3, 5, 7, 9, 11, 13, and 15, and j = I−X. Each population consists of six data points collected from six independent MPS measurements. For the case of j = X, the harmonics from sample X will be evaluated on itself, and thus, the p-values are equal to 1, indicating that these two populations are identical. As seen from the p-value heatmap in Figure 7b, all the higher harmonics from samples I and II are significantly different from the control sample X, with p-values smaller than 0.001. For samples III−V, the 3rd harmonics are significantly different from control sample X. It's worth to mention that the 7th, the 11th, and the 15th harmonics of sample VI are significantly different from control sample X with p-values smaller than 0.05, demonstrating that by using multiple higher harmonics as metrics, our MagiCoil portable device is able to detect as low as 64 nM of streptavidin (equal to 5.12 pmole). The streptavidin concentration response curves are plotted in the Supporting Information, S5 based on the 3rd, the 5th, and the 7th harmonic amplitudes from samples I to X. All the harmonic metrics show a linear dynamic range from 500 to 2000 nM.

5. DISCUSSIONS

To sum up, the higher harmonics from MPS spectra such as the 3rd to the 15th harmonics can be used as metrics to quantitatively characterize target biomarkers. By applying two-

https://dx.doi.org/10.1021/acsami.0c21040
ACS Appl. Mater. Interfaces 2021, 13, 7966−7976

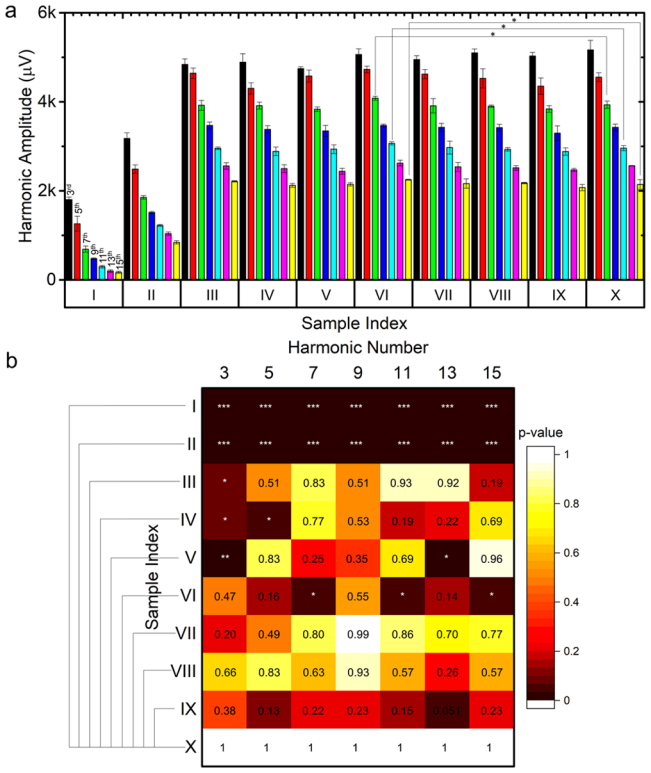

Figure 7. (a) MPS harmonics from samples I–X, monitored by the MagiCoil portable device. Error bars represent standard deviations. (b) Heatmap of p-values. *** $p < 0.001$, ** $p < 0.01$, * $p < 0.05$.

sample *t* test on samples' higher harmonics, we can achieve better sensitivity from the MagiCoil device. Since the harmonic amplitudes are proportional to amount of MNPs in the sample, thus, the MPS spectra is biased by errors introduced during MNP sample preparation. This type of error can be mitigated by using higher harmonic phase angles and harmonic ratios (e.g., amplitude ratio of the 5th over the 3rd harmonics) as metrics, which are MNP quantity-independent.[28,29,41,43] On the other hand, biological sample preparation step is the most error-prone part for all kinds of bioassays, especially for detecting the very low concentration/amount of target analytes. This type of error can be reduced by preparing multiple samples at the same concentration and performing independent determinations.

In addition to the sample incubation time, the data collection step is fully automatic and raw data is transferred to laptop in 0.54 s. At the current stage, the time domain discrete signal requires further processing such as discrete Fourier transform (DFT) to get frequency domain MPS spectra. In the future, this part of data processing can be combined in smartphone user applications.

It should be noted that the present implementation of the MPS handheld system is based on direct sampling of the MPS response followed by Fourier transform implementation in software. This implementation faces sensitivity shortcomings because of three major reasons: (1) harmonic distortions due to power amplifiers used, (2) sampling rate limitations, and (3) lower excitation frequencies used for excitations of primary and secondary coils. As can be seen from the output of the blank vial, higher harmonics are present as a result of distortion of the background sinusoidal signal due to the power amplifier currently employed. This issue only worsens by the sampling rate limitations. The currently used STMF7 microcontroller can deliver a maximum sampling frequency of 316 kSPS as implemented, but tests done with a dedicated DAQ unit (from National Instruments) show that a sampling rate greater than 500 kSPS is required for the best SNR results of the sampled MPS signal. Sensitivity of the device could also be further improved by choosing higher values for f_H and f_L excitation frequencies, and the present values used are 5 kHz and 50 Hz, respectively. The choice was made as we are presently limited by the sampling rate as choosing higher f_H and f_L would also demand for even higher sampling rates. In the future, we plan on alleviating limitations 2 and 3 (as noted above) by using a lock-in amplifier-based approach.

Furthermore, we will extend the application of detecting different types of protein biomarkers by conjugating corresponding pAb onto MNPs. Two of the major issues leading to a sensitivity hit for current implementation of the MagiCoil system are (1) unbalanced set of coils causing for a background sinusoid, which is ∼2 orders higher than the response of magnetic nanoparticles, and (2) low SNR of the signal at the ADC input, with present implementation that we are only getting an effective number of bits (ENOB) of 12 for a 24-bit ADC, which is far from the ideal. The sensitivity and robustness of the MagiCoil device can be further improved by designing a better set of balanced coils and implementing on-board lock-in modality for improvement of SNR. In addition, on-board microfluid channels are to be integrated on our MagiCoil device to (1) precisely control and process sub-microliter (sub-μL) biofluid samples, (2) reduce the incubation time by adding liquid mixing channels, and (3) concentrate all the MNPs in a smaller space where the external magnetic fields could be more uniform.

In addition, this work reports the proof-of-concept wash-free MPS bioassays on a portable device, using the streptavidin-biotin as a model. For practical applications of detecting target analytes from complex biological media such as blood, nasal swab, and sputum samples, further surface modifications on MNPs should be made to minimize or block the nonspecific bindings (NSB). Block buffers are suggested after the MNP surface functionalization step to occupy all the remaining NSB sites. Dextrans, ethanolamine, and bovine serum albumin (BSA) are frequently used as blocking reagents under these circumstances.[44−46]

Although it is in the prototype stage, we can see its great potential as a portable diagnostic device for a layperson in nonclinical settings. Many literatures have reported the flexibility of the MPS technology for a wide variety of target analytes detection. Its short assay time (typically less than 10 min) along with portability and low price make it a promising candidate for future personal healthcare. By combining this MPS technology with a lateral flow platform, researchers have reported the feasibility of multiplexed bioassays.[27,31] Table S2 in the Supporting Information qualitatively compared different diagnostic tools available in the market. At the current stage, the total cost of one MagiCoil device is approximately $300 and the user application is free of charge. Each assay uses several micrograms of iron oxide nanoparticles (less than 1 pmole of nanoparticles), and can use a few pmole of nucleic acids (i.e., DNA and RNA) and proteins (e.g., antibodies, peptides, etc.) for different applications. Therefore, the material cost per test is less than $5 and can be even lower if mass produced.

https://dx.doi.org/10.1021/acsami.0c21040
ACS Appl. Mater. Interfaces 2021, 13, 7966−7976

6. CONCLUSIONS

Herein, we have introduced a MagiCoil portable device based on the MPS technique. This portable device allows one-step, wash-free, and rapid bioassays handled by a layperson in non-laboratory settings. The capability of our MagiCoil portable device is first demonstrated in detecting different types of MNPs. The dynamic magnetic responses of different types of MNPs are monitored by our MagiCoil device and higher harmonics are summarized. It is demonstrated that the harmonic amplitudes are directly correlated to the magnetic properties of MNPs. MNPs with higher magnetic moment per volume show stronger magnetic responses as well as higher harmonic amplitudes. Based on this, we choose high moment (high magnetization per volume) SHB30 MNPs for further studies. Then, we explored the minimum amount of iron oxide MNPs that can be detected by our device. By using higher harmonics as metrics and two-sample t test, we demonstrated that this MagiCoil portable device can detect as low as 4 μg of iron oxide MNPs (equal to magnetic moment of 273.2 μemu).

We also demonstrated the feasibility of this platform for bioassay application by using the streptavidin-biotin binding system as a model. The streptavidin caused cross-linking of MNPs results in weaker dynamic magnetic responses and lower harmonic amplitudes. By analyzing the reduction of harmonic amplitudes, we can quantitatively detect the concentration/amount of target biomarkers. The streptavidin concentration response curves show a linear detection range from 500 to 2000 nM. Based on the 3rd harmonic as the sole metric, we obtained a detection limit of 128 nM (equal to 10.24 pmole). By analyzing multiple higher harmonics as metrics and using the two-sample t test, we observed a detection limit of 64 nM for streptavidin (equal to 5.12 pmole). Compared with other MPS-based bioassays reported so far, this MPS POC device is not very sensitive at this stage. To overcome this obstacle, further improvements must be made, such as higher sampling rate, higher excitation field frequency, and the introduction of a lock-in amplifier to reduce harmonic distortion.

It should be noted that the sensitivity to binding events of MNPs are affected by many parameters including the magnetic properties of MNPs (i.e., effective anisotropy and saturation magnetization) as well as the shape and size (i.e., magnetic core size and hydrodynamic size). As shown in Figure S4 in the Supporting Information, the slope of linear region from response curve is determined by the MNP's intrinsic sensitivity to bindings. In this work, we used the commercially available SHB30 MNPs for proof-of-concept, thus, we did not explore the best MNPs for an improved detection limit and a wider linear detection range. Future work should be carried out to search for MNPs with superior sensitivity to binding events.

■ ASSOCIATED CONTENT

Supporting Information

The Supporting Information is available free of charge at https://pubs.acs.org/doi/10.1021/acsami.0c21040.

3D model of the MagiCoil portable device and a smartphone application user interface, static (dc) hysteresis loops of samples A−E from Table 1, two-sample t test for samples 4 and 5 from Table 2 and Figure 3, box plots of the 5th and the 7th harmonics from samples I−X along with p-values, streptavidin concentration response curves, and comparison of the MagiCoil portable device with other diagnostic tools in the market (PDF)

■ AUTHOR INFORMATION

Corresponding Authors

Kai Wu − *Department of Electrical and Computer Engineering, University of Minnesota, Minneapolis, Minnesota 55455, United States;* orcid.org/0000-0002-9444-6112; Email: wuxx0803@umn.edu

Maxim C-J Cheeran − *Department of Veterinary Population Medicine, University of Minnesota, St. Paul, Minnesota 55108, United States*; Email: cheeran@umn.edu

Jian-Ping Wang − *Department of Electrical and Computer Engineering and Department of Chemical Engineering and Material Science, University of Minnesota, Minneapolis, Minnesota 55455, United States*; Email: jpwang@umn.edu

Authors

Vinit Kumar Chugh − *Department of Electrical and Computer Engineering, University of Minnesota, Minneapolis, Minnesota 55455, United States*

Arturo di Girolamo − *Department of Electrical and Computer Engineering, University of Minnesota, Minneapolis, Minnesota 55455, United States*

Jinming Liu − *Department of Electrical and Computer Engineering, University of Minnesota, Minneapolis, Minnesota 55455, United States;* orcid.org/0000-0002-4313-5816

Renata Saha − *Department of Electrical and Computer Engineering, University of Minnesota, Minneapolis, Minnesota 55455, United States;* orcid.org/0000-0002-0389-0083

Diqing Su − *Department of Chemical Engineering and Material Science, University of Minnesota, Minneapolis, Minnesota 55455, United States;* orcid.org/0000-0002-5790-8744

Venkatramana D. Krishna − *Department of Veterinary Population Medicine, University of Minnesota, St. Paul, Minnesota 55108, United States*

Abilash Nair − *Department of Electrical and Computer Engineering, University of Minnesota, Minneapolis, Minnesota 55455, United States*

Will Davies − *Department of Computer Science, University of Minnesota, Minneapolis, Minnesota 55455, United States*

Yongqiang Andrew Wang − *Ocean Nano Tech LLC, San Diego, California 92126, United States*

Complete contact information is available at: https://pubs.acs.org/10.1021/acsami.0c21040

Author Contributions

#K.W. and V.K.C. have contributed equally to this work.

Notes

The authors declare no competing financial interest.

■ ACKNOWLEDGMENTS

This study was financially supported by the Institute of Engineering in Medicine, the Robert F. Hartmann Endowed Chair professorship, the University of Minnesota Medical School, and the University of Minnesota Physicians and Fairview Health Services through COVID-19 Rapid Response Grant. This study was also financially supported by the U.S. Department of Agriculture-National Institute of Food and

Agriculture (NIFA) under award no. 2020-67021-31956. Research reported in this publication was supported by the National Institute Of Dental & Craniofacial Research of the National Institutes of Health under award no. R42DE030832. The content is solely the responsibility of the authors and does not necessarily represent the official views of the National Institutes of Health. Portions of this work were conducted in the Minnesota Nano Center, which is supported by the National Science Foundation through the National Nano Coordinated Infrastructure Network (NNCI) under award no. ECCS-1542202.

REFERENCES

(1) Wang, L.-J.; Chang, Y.-C.; Sun, R.; Li, L. A Multichannel Smartphone Optical Biosensor for High-Throughput Point-of-Care Diagnostics. *Biosens. Bioelectron.* **2017**, *87*, 686−692.
(2) Soni, A.; Surana, R. K.; Jha, S. K. Smartphone Based Optical Biosensor for the Detection of Urea in Saliva. *Sens. Actuators B Chem.* **2018**, *269*, 346−353.
(3) Rachim, V. P.; Chung, W.-Y. Wearable-Band Type Visible-near Infrared Optical Biosensor for Non-Invasive Blood Glucose Monitoring. *Sens. Actuators B Chem.* **2019**, *286*, 173−180.
(4) Chang, J.; Wang, X.; Wang, J.; Li, H.; Li, F. Nucleic Acid-Functionalized Metal−Organic Framework-Based Homogeneous Electrochemical Biosensor for Simultaneous Detection of Multiple Tumor Biomarkers. *Anal. Chem.* **2019**, *91*, 3604−3610.
(5) Chowdhury, A. D.; Takemura, K.; Li, T.-C.; Suzuki, T.; Park, E. Y. Electrical Pulse-Induced Electrochemical Biosensor for Hepatitis E Virus Detection. *Nat. Commun.* **2019**, *10*, 1−12.
(6) Tian, L.; Qian, K.; Qi, J.; Liu, Q.; Yao, C.; Song, W.; Wang, Y. Gold Nanoparticles Superlattices Assembly for Electrochemical Biosensor Detection of MicroRNA-21. *Biosens. Bioelectron.* **2018**, *99*, 564−570.
(7) Wang, T.; Zhou, Y.; Lei, C.; Luo, J.; Xie, S.; Pu, H. Magnetic Impedance Biosensor: A Review. *Biosens. Bioelectron.* **2017**, *90*, 418−435.
(8) Choi, J.; Gani, A. W.; Bechstein, D. J. B.; Lee, J.-R.; Utz, P. J.; Wang, S. X. Portable, One-Step, and Rapid GMR Biosensor Platform with Smartphone Interface. *Biosens. Bioelectron.* **2016**, *85*, 1−7.
(9) Wu, K.; Klein, T.; Krishna, V. D.; Su, D.; Perez, A. M.; Wang, J.-P. Portable GMR Handheld Platform for the Detection of Influenza A Virus. *ACS Sens.* **2017**, *2*, 1594−1601.
(10) Wu, K.; Liu, J.; Saha, R.; Su, D.; Krishna, V. D.; Cheeran, M. C.-J.; Wang, J.-P. Magnetic Particle Spectroscopy for Detection of Influenza A Virus Subtype H1N1. *ACS Appl. Mater. Interfaces* **2020**, *12*, 13686−13697.
(11) Ghosh Dastider, S.; Abdullah, A.; Jasim, I.; Yuksek, N. S.; Dweik, M.; Almasri, M. Low Concentration E. Coli O157: H7 Bacteria Sensing Using Microfluidic MEMS Biosensor. *Rev. Sci. Instrum.* **2018**, *89*, 125009.
(12) Abdullah, A.; Jasim, I.; Alalem, M.; Dweik, M.; Almasri, M. MEMS Based Impedance Biosensor for Rapid Detection of Low Concentrations of Foodborne Pathogens. In *2017 IEEE 30th international conference on micro electro mechanical systems (MEMS)*; IEEE: 2017; pp. 381−385.
(13) Noi, K.; Iwata, A.; Kato, F.; Ogi, H. Ultrahigh-Frequency, Wireless MEMS QCM Biosensor for Direct, Label-Free Detection of Biomarkers in a Large Amount of Contaminants. *Anal. Chem.* **2019**, *91*, 9398−9402.
(14) Yang, J.; Wang, K.; Xu, H.; Yan, W.; Jin, Q.; Cui, D. Detection Platforms for Point-of-Care Testing Based on Colorimetric, Luminescent and Magnetic Assays: A Review. *Talanta* **2019**, *202*, 96−110.
(15) Barbosa, A. I.; Reis, N. M. A Critical Insight into the Development Pipeline of Microfluidic Immunoassay Devices for the Sensitive Quantitation of Protein Biomarkers at the Point of Care. *Analyst* **2017**, *142*, 858−882.
(16) Denmark, D. J.; Bustos-Perez, X.; Swain, A.; Phan, M.-H.; Mohapatra, S.; Mohapatra, S. S. Readiness of Magnetic Nano-biosensors for Point-of-Care Commercialization. *J. Electron. Mater.* **2019**, *48*, 4749−4761.
(17) Klatman, E. L.; Jenkins, A. J.; Ahmedani, M. Y.; Ogle, G. D. Blood Glucose Meters and Test Strips: Global Market and Challenges to Access in Low-Resource Settings. *Lancet Diabetes Endocrinol.* **2019**, *7*, 150−160.
(18) Kim, H.; Chung, D.-R.; Kang, M. A New Point-of-Care Test for the Diagnosis of Infectious Diseases Based on Multiplex Lateral Flow Immunoassays. *Analyst* **2019**, *144*, 2460−2466.
(19) Neto, V. A.; Amato, V. S.; Tuon, F. F.; Gakiya, É.; de Marchi, C. R.; de Souza, R. M.; Furucho, C. R. False-Positive Results of a Rapid K39-Based Strip Test and Chagas Disease. *Int. J. Infect. Dis.* **2009**, *13*, 182−185.
(20) Lancellotti, B. V.; Bercaw, R. J.; Loomis, G. W.; Hoyt, K. P.; Avizinis, E. J.; Amador, J. A. Accuracy of Rapid Tests Used for Analysis of Advanced Onsite Wastewater Treatment System Effluent. *Water, Air, Soil Pollut.* **2016**, *227*, 310.
(21) Yang, T.; Wang, Y.-C.; Shen, C.-F.; Cheng, C.-M. *Point-of-Care RNA-Based Diagnostic Device for COVID-19*; Multidisciplinary Digital Publishing Institute: 2020.
(22) Chow, F. W.-N.; Chan, T. T.-Y.; Tam, A. R.; Zhao, S.; Yao, W.; Fung, J.; Cheng, F. K.-K.; Lo, G. C.-S.; Chu, S.; Aw-Yong, K. L.; Tang, J. Y.-M.; Tsang, C. C.; Luk, H. K.-H.; Wong, A. C.-P.; Li, K. S.-M.; Zhu, L.; He, Z.; Tam, E. W. T.; Chung, T. W.-H.; Wong, S. C. Y.; Que, T.-L.; Fung, K. S. C.; Lung, D. C.; Wu, A. K.-L.; Hung, I. F. N.; Woo, P. C.-Y.; Lau, S. K.-P. A Rapid, Simple, Inexpensive, and Mobile Colorimetric Assay COVID-19-LAMP for Mass On-Site Screening of COVID-19. *Int. J. Mol. Sci.* **2020**, *21*, 5380.
(23) Zhu, H.; Zhang, H.; Ni, S.; Korabečná, M.; Yobas, L.; Neuzil, P. The Vision of Point-of-Care PCR Tests for the COVID-19 Pandemic and Beyond. *TrAC Trends Anal. Chem.* **2020**, 115984.
(24) Udugama, B.; Kadhiresan, P.; Kozlowski, H. N.; Malekjahani, A.; Osborne, M.; Li, V. Y. C.; Chen, H.; Mubareka, S.; Gubbay, J. B.; Chan, W. C. W. Diagnosing COVID-19: The Disease and Tools for Detection. *ACS Nano* **2020**, *14*, 3822−3835.
(25) Guteneva, N. V.; Znoyko, S. L.; Orlov, A. V.; Nikitin, M. P.; Nikitin, P. I. Rapid Lateral Flow Assays Based on the Quantification of Magnetic Nanoparticle Labels for Multiplexed Immunodetection of Small Molecules: Application to the Determination of Drugs of Abuse. *Microchim. Acta* **2019**, *186*, 621.
(26) Znoyko, S. L.; Orlov, A. V.; Pushkarev, A. V.; Mochalova, E. N.; Guteneva, N. V.; Lunin, A. V.; Nikitin, M. P.; Nikitin, P. I. Ultrasensitive Quantitative Detection of Small Molecules with Rapid Lateral-Flow Assay Based on High-Affinity Bifunctional Ligand and Magnetic Nanolabels. *Anal. Chim. Acta* **2018**, *1034*, 161−167.
(27) Nikitin, M. P.; Orlov, A. V.; Znoyko, S. L.; Bragina, V. A.; Gorshkov, B. G.; Ksenevich, T. I.; Cherkasov, V. R.; Nikitin, P. I. Multiplex Biosensing with Highly Sensitive Magnetic Nanoparticle Quantification Method. *J. Magn. Magn. Mater.* **2018**, *459*, 260−264.
(28) Zhang, X.; Reeves, D. B.; Perreard, I. M.; Kett, W. C.; Griswold, K. E.; Gimi, B.; Weaver, J. B. Molecular Sensing with Magnetic Nanoparticles Using Magnetic Spectroscopy of Nanoparticle Brownian Motion. *Biosens. Bioelectron.* **2013**, *50*, 441−446.
(29) Wu, K.; Liu, J.; Su, D.; Saha, R.; Wang, J.-P. Magnetic Nanoparticle Relaxation Dynamics-Based Magnetic Particle Spectroscopy for Rapid and Wash-Free Molecular Sensing. *ACS Appl. Mater. Interfaces* **2019**, *11*, 22979−22986.
(30) Wu, K.; Su, D.; Saha, R.; Wong, D.; Wang, J.-P. Magnetic Particle Spectroscopy-Based Bioassays: Methods, Applications, Advances, and Future Opportunities. *J. Phys. Appl. Phys.* **2019**, *52*, 173001.
(31) Orlov, A. V.; Znoyko, S. L.; Cherkasov, V. R.; Nikitin, M. P.; Nikitin, P. I. Multiplex Biosensing Based on Highly Sensitive Magnetic Nanolabel Quantification: Rapid Detection of Botulinum Neurotoxins A, B, and E in Liquids. *Anal. Chem.* **2016**, *88*, 10419−10426.

https://dx.doi.org/10.1021/acsami.0c21040
ACS Appl. Mater. Interfaces 2021, 13, 7966−7976

(32) Znoyko, S. L.; Orlov, A. V.; Bragina, V. A.; Nikitin, M. P.; Nikitin, P. I. Nanomagnetic Lateral Flow Assay for High-Precision Quantification of Diagnostically Relevant Concentrations of Serum TSH. *Talanta* **2020**, 120961.
(33) Bragina, V. A.; Znoyko, S. L.; Orlov, A. V.; Pushkarev, A. V.; Nikitin, M. P.; Nikitin, P. I. Analytical Platform with Selectable Assay Parameters Based on Three Functions of Magnetic Nanoparticles: Demonstration of Highly Sensitive Rapid Quantitation of Staphylococcal Enterotoxin B in Food. *Anal. Chem.* **2019**, *91*, 9852−9857.
(34) Pietschmann, J.; Voepel, N.; Spiegel, H.; Krause, H.-J.; Schroeper, F. Brief Communication: Magnetic Immuno-Detection of SARS-CoV-2 Specific Antibodies. *bioRxiv* **2020**, DOI: 10.1101/2020.06.02.131102.
(35) Akiyoshi, K.; Yoshida, T.; Sasayama, T.; Elrefai, A. L.; Hara, M.; Enpuku, K. Wash-Free Detection of Biological Target Using Cluster Formation of Magnetic Markers. *J. Magn. Magn. Mater.* **2020**, *500*, 166356.
(36) Gordon-Wylie, S. W.; Ness, D. B.; Shi, Y.; Mirza, S. K.; Paulsen, K. D.; Weaver, J. B. Measuring Protein Biomarker Concentrations Using Antibody Tagged Magnetic Nanoparticles. *Biomed. Phys. Eng. Express* **2020**, *6*, No. 065025.
(37) Zhong, J.; Schilling, M.; Ludwig, F. Magnetic Nanoparticle-Based Biomolecule Imaging with a Scanning Magnetic Particle Spectrometer. *Nanotechnology* **2020**, *31*, 225101.
(38) Chugh, V. K.; Wu, K.; Nair, A.; di Girolamo, A.; Schealler, J.; Vuong, H.; Davies, W.; Wall, A.; Whitely, E.; Saha, R. Magnetic Particle Spectroscopy-Based Handheld Device for Wash-Free, Easy-to-Use, and Solution-Phase Immunoassay Applications. In *2020 Design of Medical Devices Conference*; American Society of Mechanical Engineers Digital Collection: 2020.
(39) Krause, H.-J.; Wolters, N.; Zhang, Y.; Offenhäusser, A.; Miethe, P.; Meyer, M. H. F.; Hartmann, M.; Keusgen, M. Magnetic Particle Detection by Frequency Mixing for Immunoassay Applications. *J. Magn. Magn. Mater.* **2007**, *311*, 436−444.
(40) Nikitin, P. I.; Vetoshko, P. M.; Ksenevich, T. I. New Type of Biosensor Based on Magnetic Nanoparticle Detection. *J. Magn. Magn. Mater.* **2007**, *311*, 445−449.
(41) Rauwerdink, A. M.; Weaver, J. B. Harmonic Phase Angle as a Concentration-Independent Measure of Nanoparticle Dynamics. *Med. Phys.* **2010**, *37*, 2587−2592.
(42) Chung, S.-H.; Hoffmann, A.; Guslienko, K.; Bader, S. D.; Liu, C.; Kay, B.; Makowski, L.; Chen, L. Biological Sensing with Magnetic Nanoparticles Using Brownian Relaxation. *J. Appl. Phys.* **2005**, *97*, 10R101.
(43) Shi, Y.; Khurshid, H.; Ness, D. B.; Weaver, J. B. Harmonic Phase Angles Used for Nanoparticle Sensing. *Phys. Med. Biol.* **2017**, *62*, 8102.
(44) Balcer, H. I.; Spiker, J. O.; Kang, K. A. Effects of Blocking Buffers and Plasma Proteins on the Protein C Biosensor Performance. In *Oxygen Transport to Tissue XXIV*; Springer: 2003; pp. 133−141, DOI: 10.1007/978-1-4615-0075-9_13.
(45) Contreras-Naranjo, J.; Aguilar, O. Suppressing Non-Specific Binding of Proteins onto Electrode Surfaces in the Development of Electrochemical Immunosensors. *Biosensors* **2019**, *9*, 15.
(46) Schneider, C. S.; Bhargav, A. G.; Perez, J. G.; Wadajkar, A. S.; Winkles, J. A.; Woodworth, G. F.; Kim, A. J. Surface Plasmon Resonance as a High Throughput Method to Evaluate Specific and Non-Specific Binding of Nanotherapeutics. *J. Controlled Release* **2015**, *219*, 331−344.

https://dx.doi.org/10.1021/acsami.0c21040
ACS Appl. Mater. Interfaces 2021, 13, 7966−7976